Journal of Hazardous Materials 183 (2010) 482–489

Contents lists available at ScienceDirect

Journal of Hazardous Materials

journal homepage: www.elsevier.com/locate/jhazmat

Kinetic analysis and modeling of oleate and ethanol stimulated uranium (VI) bio-reduction in contaminated sediments under sulfate reduction conditions

Fan Zhang[a,*,1], Wei-Min Wu[b,1], Jack C. Parker[c], Tonia Mehlhorn[d], Shelly D. Kelly[e], Kenneth M. Kemner[e], Gengxin Zhang[a], Christopher Schadt[d], Scott C. Brooks[d], Craig S. Criddle[b], David B. Watson[d], Philip M. Jardine[f]

[a] Key Laboratory of Tibetan Environment Changes and Land Surface Processes, Institute of Tibetan Plateau Research, Chinese Academy of Sciences, P.O. Box 2871, Beijing 100085, China
[b] Department of Civil and Environmental Engineering, Stanford University, Stanford, CA 94305, USA
[c] Department of Civil and Environmental Engineering, University of Tennessee, Knoxville, TN 37996, USA
[d] Environmental Sciences Division, Oak Ridge National Laboratory, Oak Ridge, TN 37831, USA
[e] Biosciences Division, Argonne National Laboratory, Argonne, IL 60439, USA
[f] Biosystems Engineering and Soil Science Department, University of Tennessee, Knoxville, TN 37996, USA

ARTICLE INFO

Article history:
Received 8 February 2010
Received in revised form 29 May 2010
Accepted 12 July 2010
Available online 21 July 2010

Keywords:
Bio-stimulation
Microbial reduction
Intermediate products
Acetate
Hydrogen
Simulate

ABSTRACT

Microcosm tests with uranium contaminated sediments were performed to explore the feasibility of using oleate as a slow-release electron donor for U(VI) reduction in comparison to ethanol. Oleate degradation proceeded more slowly than ethanol with acetate produced as an intermediate for both electron donors under a range of initial sulfate concentrations. A kinetic microbial reduction model was developed and implemented to describe and compare the reduction of sulfate and U(VI) with oleate or ethanol. The reaction path model considers detailed oleate/ethanol degradation and the production and consumption of intermediates, acetate and hydrogen. Although significant assumptions are made, the model tracked the major trend of sulfate and U(VI) reduction and describes the successive production and consumption of acetate, concurrent with microbial reduction of aqueous sulfate and U(VI) species. The model results imply that the overall rate of U(VI) bioreduction is influenced by both the degradation rate of organic substrates and consumption rate of intermediate products.

© 2010 Elsevier B.V. All rights reserved.

1. Introduction

In situ anaerobic bioremediation has been used for the remediation of a variety of subsurface contaminants including chlorinated aliphatic hydrocarbons, perchlorate, chromate and radionuclides such as uranium [1,2]. Microbial reduction of soluble uranium (VI) to sparingly soluble and immobile U(IV) is one promising strategy to limit subsurface uranium migration [3]. The process is often mediated by iron-reducing bacteria (FeRB), sulfate-reducing bacteria (SRB), and a diverse range of other bacteria able to convert U(VI) to U(IV) species or uraninite or $UO_2(s)$ in the presence of electron donor sources [4]. Various fast-degrading electron donor sources have been tested for U(VI) reduction in contaminated sediments *in situ*, including ethanol, acetate and glucose [5–8]. Using weekly ethanol injection, uranium concentrations below US EPA drinking water standard (<0.03 mg/l) were achieved and maintained in a highly contaminated area at the US DOE Oak Ridge site [7]. Relatively rapid U(VI) attenuation was observed associated with ethanol degradation and acetate accumulation:

$$C_2H_6O + H_2O \rightarrow C_2H_3O_2^- + 2H_2 + H^+ \quad (1)$$

To maintain anaerobic, reducing conditions, frequent ethanol delivery is required. Field experience with bioremediation of chlorinated solvents has demonstrated that the delivery of a readily metabolized substrate can result in clogging due to over-growth of microbes near the injection port that limits efficient distribution of electron donor into the contaminated area.

Slow-release electron donor sources (such as oleate and edible oil) that have a relatively high energy density have been considered as alternative electron donor sources for bioreduction of chlorinated solvents [9,10]. The slow degradation of substrates can allow high penetration into the subsurface. Oleic acid is a monounsaturated omega-9 fatty acid found in various animal and vegetable oil sources and also a major long-chain fatty acid (FA) in wastewaters as the product of lipid hydrolysis [11]. Because oleate is a major long-chain FA in vegetable oil, it will be produced as the oil is hydrolyzed during biodegradation. In the presence of Ca^{2+} ions,

* Corresponding author. Tel.: +86 10 62849383; fax: +86 10 62849886.
E-mail address: zhangfan@itpcas.ac.cn (F. Zhang).
[1] Fan Zhang and Wei-Min Wu contributed equally to this work.

0304-3894/$ – see front matter © 2010 Elsevier B.V. All rights reserved.
doi:10.1016/j.jhazmat.2010.07.049

oleate forms calcium–oleate precipitates:

$$2C_{18}H_{33}O_2^- + Ca^{2+} \rightarrow Ca(C_{18}H_{33}O_2)_2\downarrow \quad (2)$$

If oleic acid were delivered to subsurface, the precipitated calcium–oleate could be trapped or attached to subsurface sediment and serve as a long-term energy source for microbial growth and bioreduction. The anaerobic degradation of oleate can be performed by syntrophic consortia composed of butyrate-degraders (e.g. *Syntrophomonas* spp.) together with H_2-utilizing methanogens or SRB, with acetate as an intermediate [12,13]:

$$C_{18}H_{33}O_2^- + 16H_2O \rightarrow 9C_2H_3O_2^- + 15H_2 + 8H^+ \quad (3)$$

In this reaction, hydrogen must be maintained at a low level (a few Pa or lower partial pressure) via consumption by methanogens or SRB for the reaction to be thermodynamically favorable. During oleate degradation, acetate was accumulated as a major product, while other FAs were not found as degradation products [13]. Recently, we found that the degradation of oleate can also be performed by sulfate-reducing *Desulforegula conservatrix* – like bacteria, which degrades other long-chain FAs [14]. Oleate and its degradation product acetate and hydrogen could serve as electron donor source for U(VI) reduction. To date, however, no report has been published about the use of oleate as an electron donor source for U(VI) reduction.

In field settings, groundwater geochemistry may significantly influence bioremediation results. At US DOE uranium contaminated sites, sulfate is presented in groundwater and U(VI) reduction is likely performed under sulfate-reducing condition with H_2-producing substrate like ethanol [15,16]. The pilot field study at the Oak Ridge site indicated that SRB were abundant [6]. SRB use sulfate as an electron acceptor for the dissimilation of various organic matters and hydrogen to support their metabolic activity [17,18]. SRB are also capable of reducing various inorganic ions in aqueous solution such as iron (III), manganese (IV), uranium (VI), and technetium (VII), etc [18]. Under sulfate-reducing conditions, accelerated dissolution of the iron oxides may be due to redox-reactions between ferric iron and sulfides [19]. The impact of sulfate on field scale U(VI) reduction has been studied previously [20,21]. In addition, the end products of sulfate reduction, hydrogen sulfide and sulfide (as FeS), also abiotically reduce U(VI) to U(IV) but the presence of bicarbonate and neutral or high pH may inhibit the reduction [22,23].

Understanding bioreduction processes is crucial to successfully predict long-term fate of environmental uranium [24]. Models for the reduction of metals and radionuclides by SRB can be used to develop and design treatment systems employing SRB for bioremediation [18]. Modeling U(VI) bioreduction requires the consideration of uranium aqueous chemistry, uranium sorption/desorption, and bioreactive kinetics [25]. Microbial U(VI) reduction have been described by several investigators using various formulations, such as first-order kinetics [18,26], and more widely used Michaelis–Menten or Monod kinetics [18,25,27,28]. Previous modeling efforts have made a variety of simplifying assumptions, for example, not including aqueous complexation and sorption reaction of uranium [18,27]. Other investigators have lumped bioreduction kinetics without considering production and consumption of intermediates [25].

In this study, we used microcosms to study U(VI) reduction with oleate in comparison to ethanol at different initial sulfate concentrations. Kinetic microbial reduction model incorporated with equilibrium aqueous complexation and surface complexation reactions was developed to describe the degradation of oleate or ethanol associated with U(VI) reduction to U(IV). Construction of the reaction path model and simulation of the tests provided insight to the bioreduction processes and identified the rate limiting factors.

2. Materials and methods

2.1. Microcosm test

Microcosms were established in 158 ml serum bottles using groundwater and sediment from Area 2 of OR-IFRC site (Fig. S1 supplementary data) and incubated at ambient temperature (22–24 °C). Groundwater from well FW231-2 was used and had the following composition: pH 6.73; nitrate, 1.37 mM; sulfate, 1.14 mM; Ca, 2.60 mM; U(VI), 4.87 μM; COD and nitrite, 0. Sediment samples from sampling cores FB107 and FB109 were mixed for use in the microcosms. Soil-saprolite material in the samples exhibited a particle size ranging from 0.15 to 1.0 mm and contained 0.649 mg/g U(VI); 49 mg/g HCl extractable iron that includes 18.28 mg/g Fe(II); and 18.6 mg/g COD. Microcosms were established in an anaerobic glovebag by mixing 8.51 g (dry weight) sediment with 130 ml amended groundwater (Table 1). The microcosms were then sealed with butyl rubber stoppers and aluminum caps for 5 weeks.

Experimental replicates contained either sodium oleate or ethanol as electron donor plus various levels of sulfate (from Na_2SO_4) amendment. Negative controls received neither electron donor nor sulfate. Oleate or ethanol was added to the microcosm to achieve electron donor level of 720 mg COD/l (0.92 mM of oleate or 9 mM of ethanol) for a theoretical hydrogen yield of 1.794 and 2.34 mmole per bottle for oleate and ethanol, respectively (Eqs. (1) and (3)). Microcosms were mixed by shaking and allowed to settle for 12 h before sampling the aqueous phase at time zero. Subsequently, the microcosms were incubated without shaking to simulate conditions influenced only by diffusivity. Samples (about 1.5 ml each time) were withdrawn periodically for the quantification of U(VI), pH, COD, acetate and sulfate in the aqueous phase. The change of volume of aqueous phase was recorded based on weight change of each microcosm before and after sampling. At the end of the test, headspace gas composition was analyzed and sulfide, Fe(II) and alkalinity in aqueous phase were measured. Sediment samples were also withdrawn for the analysis of U speciation and iron (II) content.

2.2. Analytical methods

The source and quality of chemicals used and analytical methods have been described in detail previously [6,7]. Uranium(VI) in aqueous phase was measured using a kinetic phosphorescence KPA-11analyzer (Chemchek Instruments, Richland,WA). Anions (acetate, NO_3^-, Cl^-, and SO_4^{2-}) were analyzed with an ion chromatograph equipped with an IonPac AS-14 analytical column and an AG-14 guard column (Dionex DX-120, Sunnyvale, CA). Cations (Ca, Fe, Mn, Mg, U, K, Na, etc.) were determined using an inductively coupled plasma mass spectrometer (ICPMS) (Perkin Elmer ELAN 6100). The oxidation state of U in sediments was determined by U L_3-edge XANES [29,30]. The Fe(II) and Fe contents in the solid phase was determined by extraction of sediment sample (30–50 mg dry weight) using 1.5 ml of HCl (6N) for 24 h. Aqueous Fe(II), total Fe, sulfide and COD was measured colorimetrically using a HACH DR 2000 spectrophotometer (Hach Chemical, Loveland, CO). Methane and hydrogen in gas phase was measured by gas chromatography as described by Spalding and Watson (2006).

2.3. Electron balance estimation

At the end of the test, electron balance was estimated based on available electrons from complete oxidation of oleate or ethanol, electrons required for electron acceptor consumption and electrons in intermediates of oleate or ethanol degradation. The half reactions for electron transfer are based on those published previously

Table 1
Chemical composition in aqueous phase before bioreduction with oletate or ethanol.

Microcosm	Control	Oleate			Ethanol	
		A1	A2	A3	B1	B2
Substrate	No	Oleate	Oleate	Oleate	Ethanol	Ethanol
Concentration, mM[a]	no	0.92	0.92	0.92	9.0	9.0
Added SO_4^{2-}, mM	no	no	3.85	7.70	no	3.85
pH	7.13	6.89	7.00	7.04	6.85	6.92
HCO_3^-, mM	6.60	6.60	6.60	6.60	6.60	6.60
SO_4^{2-}, mM	1.09	1.09	4.92	8.58	1.07	4.89
U, μM	14.9	14.5	23.5	27.3	14.9	22.8
Fe, mM	0.0041	0.0034	0.0047	0.0035	0.0040	0.0039
Na^+, mM	0.51	0.61	7.81	15	0.51	8.03
K^+, mM	0.16	0.15	0.12	0.13	0.11	0.13
Ca^{2+}, mM	2.80	2.80	2.88	3.03	2.83	2.88
Mg^{2+}, mM	0.76	0.76	0.77	0.81	0.77	0.78
Mn^{2+}, mM	0.029	0.030	0.032	0.032	0.027	0.029
$CaUO_2(CO_3)_3^{2-}$ in U, %[b]	19.7	19.7	19.3	18.6	19.7	19.3
$Ca_2UO_2(CO_3)_3$ in U, %[b]	80.0	80.0	80.4	81.1	80.0	80.4
H_2 source available (mmole)[b]	No	1.794	1.794	1.794	2.34	2.34

[a] The COD concentration of ethanol or oleate was 720 mg/l (COD/electron = 8 mg/mmole).
[b] Calculated.

[2,31,32] at pH 7.0 (Table 2). The half reactions include oleate oxidation, ethanol oxidation, acetate oxidation and hydrogen oxidation. Both hydrogen and acetate are considered as intermediates of oleate or ethanol degradation. Major reactions involved in electron acceptor consumption include nitrate reduction, sulfate reduction, Fe(III) reduction, CO_2 reduction (methanogenesis) and U(VI) reduction to U(IV).

2.4. Modeling tools

The computer code HydroGeoChem v5.0 (HGC5) [33,34] is a comprehensive model for water flow and reactive transport. The biogeochemical reactive transport module of HGC5 was used to calculate concentration changes and distributions of various species. The program is designed for generic biogeochemical reaction networks, which may include both equilibrium and kinetic reactions with user specified formulations [35]. HGC5 was coupled with the nonlinear inversion code PEST [36] to automate calibration of specified model coefficients from measured data.

2.5. Basic geochemistry model

At the OR-IFRC site, uranium in contaminated sediment is mainly present as uranyl which is predominantly bound to monodentate phosphorus and bidentate carbon ligands [29]. The basic geochemistry model includes uranium aqueous complexation reactions [37–39] (Table S1 of supplementary data) and surface complexation reactions for uranium sorption [40] (Table S2 of supplementary data):

$$S(OH)_2 + UO_2^{2+} \overset{K_{e1}}{\leftrightarrows} SO_2UO_2 + 2H^+ \quad (4)$$

$$W(OH)_2 + UO_2^{2+} \overset{K_{e2}}{\leftrightarrows} WO_2UO_2 + 2H^+ \quad (5)$$

$$S(OH)_2 + UO_2^{2+} + CO_3^{2-} \overset{K_{e3}}{\leftrightarrows} SO_2UO_2CO_3^{2-} + 2H^+ \quad (6)$$

$$W(OH)_2 + UO_2^{2+}CO_3^{2-} \overset{K_{e4}}{\leftrightarrows} WO_2UO_2CO_3^{2-} + 2H^+ \quad (7)$$

where UO_2^{2+} is a uranyl species in aqueous phase, S and W denote strong and weak surface binding sites, respectively, and K_{e1}, K_{e2}, K_{e3}, and K_{e4} are equilibrium coefficients for the individual reactions. Previously, we determined the values for $\log K_{e1}$, $\log K_{e2}$, $\log K_{e3}$, and $\log K_{e4}$ to be −2.64, −6.84, −13.68, −17.28, respectively, and strong and weak sorbing site densities to be 0.0018 mole sites/mole Fe(III) and 0.8732 mole sites/mole Fe(III), respectively, for the sediment from the studied site [41]. In addition, a surface complexation model describing sulfate sorption [42] was introduced to model.

$$XOH + H^+ + SO_4^{2-} \overset{K_{e5}}{\leftrightarrows} XSO_4^- + H_2O \quad (8)$$

where X denotes both strong and weak surface binding sites and $\log K_{e5}$ is equilibrium coefficient that was calibrated from initial aqueous composition data (Table 1).

A previous study showed that at low pH, U(VI) sorption is mainly due to cation exchange involving the U(VI) species represented by $UO2^{2+}$, while at higher pH, sorption of U(VI) is dominated by anionic uranyl–carbonate species [16]. Therefore, cation exchange of U(VI) is omitted in this study for microcosm tests performed under pH ∼ 7.

2.6. Reaction pathway model

A kinetic microbial reduction model incorporated with the basic geochemistry model were developed to describe the sulfate and

Table 2
Half reactions for electron transfer associated with bioreduction with oletate or ethanol.

No.	Processes	Half reactions for electron transfer
1	Oleate oxidation	$C_{18}H_{33}O_2^- + 43H_2O \rightarrow 9CO_2 + 9HCO_3^- + 110H^+ + 102e^-$
2	Ethanol oxidation	$C_2H_6O + 3H_2O \rightarrow 2CO_2 + 12H^+ + 12e^-$
3	Acetate oxidation	$CH_3CO_2^- + 3H_2O \rightarrow CO_2 + HCO_3^- + 8H^+ + 8e^-$
4	Hydrogen oxidation	$H_2 \rightarrow 2H^+ + 2e^-$
5	Denitrification of nitrate	$NO_3^- + 6H^+ + 5e^- \rightarrow 0.5N_2 + 3H_2O$
6	Sulfate reduction	$SO_4^{2-} + 9.5H^+ + 8e^- \rightarrow 0.5H_2S + 0.5HS^- + 4H_2O$
7	Fe(III) reduction	$Fe^{3+} + e^- \rightarrow Fe^{2+}$
8	Methanogenesis (CO_2 reduction)	$CO_2 + 8H^+ + 8e^- \rightarrow CH_4 + 2H_2O$
9	U(VI) reduction to U(IV)	$UO_2(CO_3)_3^{4-} + 3H^+ + 2e^- \rightarrow UO_{2(s)} + 3HCO_3^-$

uranium reduction stimulated by oleate or ethanol. The reaction path model considers detailed oleate/ethanol degradation and the production and consumption of intermediates, acetate and hydrogen. Ammonium was considered as a nitrogen source for microbial growth. In addition to the aqueous complexation and surface complexation reactions specified in the basic geochemistry model, six kinetic bioreactions are included in the model. First, oleate degradation

$$C_{18}H_{33}O_2^- + 16H_2O \rightarrow 9C_2H_3O_2^- + 15H_2 + 8H^+, \quad R_1 = K_1 C_{\text{oleate}} \tag{9}$$

or ethanol degradation

$$C_2H_6O_2 + H_2O \rightarrow C_2H_3O_2^- + 2H_2 + H^+, \quad R_1 = K_1 C_{\text{ethanol}} \tag{10}$$

Second, sulfate reduction by acetate

$$0.125C_2H_3O_2^- + 0.1125SO_4^{2-} + 0.00435NH_4^+ + 0.16875H^+ \rightarrow 0.00435C_5H_7O_2N + 0.05625H_2S + 0.05625HS^- + 0.1033CO_2 + 0.125HCO_3^- + 0.1098H_2O \tag{11}$$

$$R_2 = K_2 \cdot \frac{C_{\text{acetate}}}{K_{\text{acetate}} + C_{\text{acetate}}} \cdot \frac{C_{SO_4}}{K_{SO_4} + C_{SO_4}}$$

Third, sulfate reduction by hydrogen

$$0.5H_2 + 0.1125SO_4^{2-} + 0.00435NH_4^+ + 0.16875H^+ + 0.02174CO_2 \rightarrow 0.00435C_5H_7O_2N + 0.05625H_2S + 0.05625HS^- + 0.4848H_2O \tag{12}$$

$$R_3 = K_3 \cdot \frac{C_{H_2}}{K_{H_2} + C_{H_2}} \cdot \frac{C_{SO_4}}{K_{SO_4} + C_{SO_4}}$$

Fourth, U(VI) reduction by acetate

$$0.125C_2H_3O_2^- + 0.45UO_2(CO_3)_3^{4-} + 0.00435NH_4^+ + 0.45H^+ + 0.3402H_2O \rightarrow 0.00435C_5H_7O_2N + 0.45UO_{2(s)} + 0.1033CO_2 + 1.475HCO_3^- \tag{13}$$

$$R_4 = K_4 \cdot \frac{C_{\text{acetate}}}{K_{\text{acetate}} + C_{\text{acetate}}} \cdot \frac{C_{U(VI)}}{K_{U(VI)} + C_{U(VI)}}$$

Fifth, U(VI) reduction by hydrogen

$$0.5H_2 + 0.45UO_2(CO_3)_3^{4-} + 0.00435NH_4^+ + 0.45H^+ + 0.02174CO_2 \rightarrow 0.03478H_2O + 0.00435C_5H_7O_2N + 0.45UO_{2(s)} + 1.35HCO_3^- \tag{14}$$

$$R_5 = K_5 \cdot \frac{C_{H_2}}{K_{H_2} + C_{H_2}} \cdot \frac{C_{U(VI)}}{K_{U(VI)} + C_{U(VI)}}$$

where R_1 is degradation rate of oleate for oleate amended system or degradation rate of acetate for acetate amended system; R_2 and R_3 are rate of sulfate reduction by acetate and hydrogen, respectively; and R_4 and R_5 are rate of U(VI) reduction by acetate and hydrogen, respectively. R_2 through R_5 are formulated by a dual Monod rate law. K_1 is the rate constant for degradation of oleate or acetate; K_2 and K_3 are the maximum specific rate of substrate utilization for sulfate; and K_4 and K_5 are the maximum specific rate of substrate utilization for U(VI), $K_{\text{acetate}} = 0.07$ mM [43], $K_{H_2} = 141$ pa [44], $K_{SO_4} = 0.01$ mM [25] and $K_{U(VI)} = 0.5$ mM [25] are half saturation coefficient for acetate, hydrogen, sulfate and U(VI), respectively.

3. Results and discussion

3.1. Initial aqueous composition simulation

Nitrate was not detected in all microcosms in the samples from all microcosms at time zero. It was consumed due to microbial activity probably using sediment organic matter (as 18.6 mg COD/g). In contrast, constant sulfate concentration in the control indicated no sulfate reduction in the absence of electron donor amendment (Fig. S2). In the control microcosm after mixing the sediment with groundwater, aqueous U(VI) concentration increased gradually from 12.1 to 15.2 μM over the first 5 weeks due to desorption of U(VI) from sediments (Fig. 1 and Fig. S2, supplementary data). Microcosms receiving sulfate supplement (A2, A3, and B2) showed increased uranium concentration (Table 1). Oleate or ethanol was introduced to the tested microcosms after U(VI) concentrations reach steady level after 5 weeks at static condition. The steady state aqueous composition was simulated using the basic geochemistry model including aqueous complexation and surface complexation reactions. The equilibrium coefficient of the sulfate surface complexation reaction $\log K_{e5}$ (Eq. (8)), which directly affects the amount of sulfate sorption and indirectly affects the amount of competing uranium and carbonate sorption, was calibrated to be 8.08 ± 0.24 to achieve the best fit of the aqueous sulfate and uranium concentrations and alkalinity. The amount of total carbonate and sulfate in the systems of mixed sediments and groundwater were not measured and thus estimated together with $\log K_{e5}$. Total of dissolved and sorbed carbonate was estimated to be 18.7 ± 0.4 mM. The total sulfate including dissolved and sorbed was estimated to be 1.44 ± 0.22 mM. The simulated sulfate concentrations are close to those measured in microcosms when desorption of the sorbed fraction is taken into account (Table 1). The dominant aqueous U(VI) species was the calcium–uranyl–carbonate complex, $Ca_2UO_2(CO_3)_3$ (Table 1).

Table 3
Chemical composition at the end of test and relative electron recoveries for major reactions (as %).

Microcosm	Oleate			Ethanol	
	A1	A2	A3	B1	B2
Substrate	Oleate	Oleate	Oleate	Ethanol	Ethanol
Initial SO_4^{2-}, mM	1.09	4.92	8.58	1.07	4.89
pH	7.01	7.14	7.46	7.02	7.40
HCO_3^-, mM	14.5	17.9	25.4	13.3	15.0
U, μM	0.95	1.89	2.33	0.42	2.07
S^{2-}, mM	0.0078	0.0039	0.0141	0.0023	0.0102
Fe^{2+}, mM	0.290	0.058	0.0095	0.18	0.022
U(IV)/total U in solids, %	37	61	65	56	65
Fe(II) generated, mmole	1.08	1.64	1.76	1.12	1.58
CH_4, mmole	0.817	0.539	0.10	0.842	0.425
Electron recovery, %					
CH_4 production	75.0	40.25	7.38	75.37	35.02
Sulfate reduction	12.01	44.09	76.03	11.49	48.43
Fe(II) reduction	12.78	15.38	16.28	12.82	16.30
U(IV) reduction	0.21	0.28	0.30	0.31	0.33

Note: Sulfate and acetate were not detected in the microcosms except for control at the end of the test (day 180). U speciation was analyzed by XANES. Fe(II) generated was calculated based on the difference between total Fe(II) in the microcosm with amended electron donor and that in control.

3.2. Electron balance

The changes in aqueous concentrations of U(VI), sulfate and acetate in the microcosms over a 100-day incubation are illustrated in Fig. 1 and the result for mass balance is presented in Table 3. Removal of aqueous U(VI) was observed with the addition of either oleate or ethanol (Fig. 1a1–a3). The reduction of U(VI) to U(IV) was confirmed by XANES analysis of the sediments. At the end of the test less U(VI) was reduced to U(IV) using oleate than ethanol when normalized on a COD basis (37% in A1 versus 56% in B1 and 61% in A2 versus 65% in B2). The extent of U(VI) reduced was likely related to hydrogen source available via substrate degradation (1.794 versus 2.34 mmole per bottle for oleate and ethanol respectively as shown in Table 1). Removal of aqueous sulfate was also observed (Fig. 1b1–b3). Higher initial sulfate concentration resulted in more U(IV) in aqueous phase at the beginning of the experiment (Table 3). According to the half reactions for electron transfer (Table 2), the percentage of electron recovery was estimated based on the electrons for the production of CH_4, Fe(II) and U(IV) and inferred S(II) from sulfate loss (Table 3). Denitrification was not counted in this study since nitrate was consumed before electron donor was added. The electrons used for U(VI) reduction was very limited (<0.4%). More than 50% of electrons were used for sulfate and Fe(III) reduction, to produce reduced products sulfide and Fe(II) compounds in the presence of high sulfate (A2, A3 and B2). But most electrons (>75%) were used for methane production in the presence of low

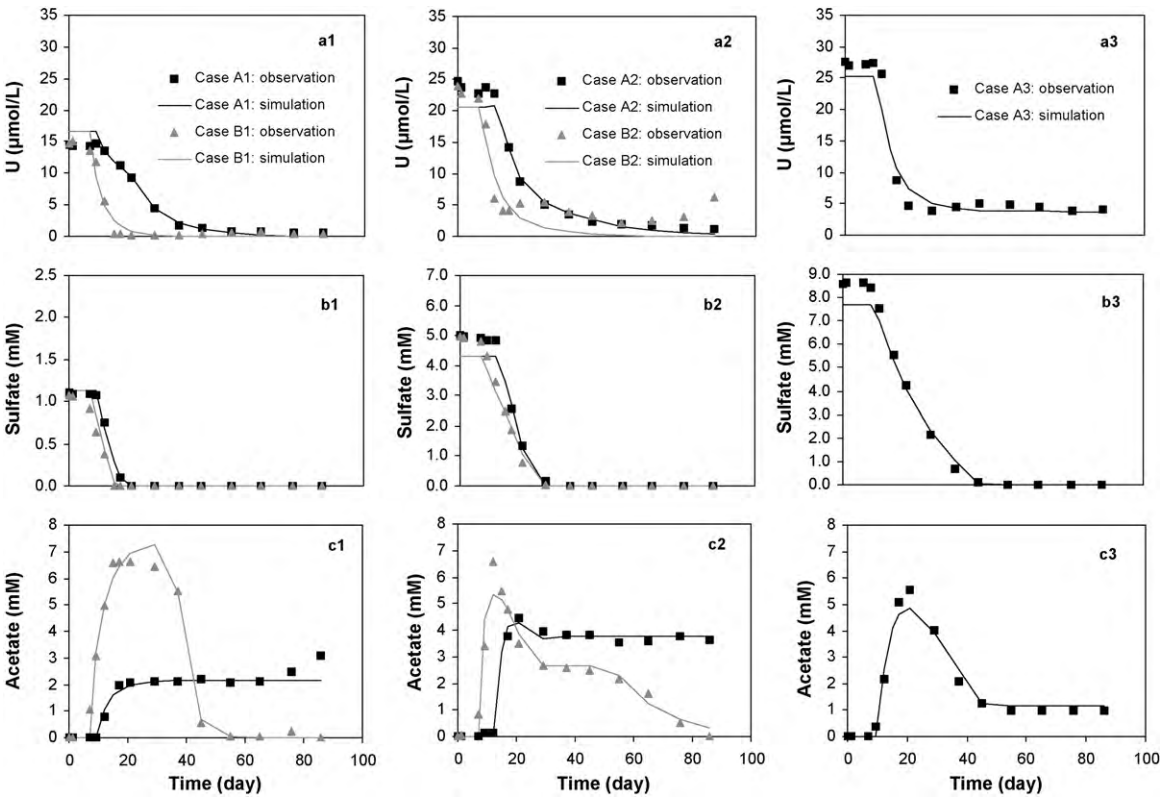

Fig. 1. Evolution of aqueous U(VI), sulfate, and acetate concentrations during oleate and ethanol stimulated bio-reduction and reaction pathway model simulations. Observations and simulations are represented by dots and curves, separately. Oleate and ethanol tests are shown in black and grey, respectively. a1–a3, b1–b3 and c1–c3 show concentration of dissolved U, sulfate and acetate, respectively. a1, b1, and c1 describe tests with initial sulfate concentration of 1.09 mM, a2, b2, and c2 describe tests with initial sulfate concentration of 4.92 mM, and a3, b3, and c3 describe tests with initial sulfate concentration of 8.58 mM.

sulfate (A1 and B1). At higher initial sulfate concentration more electron donor was consumed by SRB and more U(VI) was reduced to U(IV) while fewer electrons were used for methane production. Less than 17% of electrons were used in Fe(III) reduction with no clear trend in response to sulfate amendment. We assumed that significant portion of the Fe(III) reduction may be due to chemical reduction by biogenic sulfide [19]. Complete reduction of Fe(III) solids in sediment matrix is impossible due to poor availability. Our other test indicated that a large fraction of Fe(III) could remained in the sediments over months under anaerobic condition [30]. A separate microcosm study showed that at the population of FeRB was in much lower abundances than species known to oxidize long-chain fatty acids and reduce sulfate and U(VI) in the presence of sulfate [25]. Therefore, electrons from degradation of oleate or ethanol that were consumed by bioreduction of Fe(III) to Fe(II) are neglected in the modeling.

3.3. *Oleate/ethanol degradation and sulfate reduction in microcosms.*

Oleate degradation was indirectly monitored by measuring production of the intermediate breakdown product acetate [32]. Acetate was also monitored in ethanol amended microcosms. The lag period for oleate degradation (9 days) was longer for than ethanol degradation (<6 days) (Fig. 1c1–c3). Acetate was more rapidly produced in ethanol amended microcosms. During the same period, sulfate concentration started decreasing. The produced acetate was then partially consumed and stabilized after sulfate was completely depleted. Under the same initial sulfate concentration, acetate production and sulfate removal occurred earlier and more rapidly with ethanol than oleate. For ethanol amended microcosms, the initial sulfate concentration did not influence the peak level of acetate likely due to the fact that ethanol can be degraded via either sulfate reduction or syntrophic acetogenesis (Wu et al., 1991). For oleate amended microcosms, the sulfate concentration influenced the peak level (Fig. 1). Lower peak concentrations of acetate were observed with lower initial sulfate concentration, suggesting that oleate degradation was more dependent on sulfate reduction during initial 30 days. For ethanol amended microcosms B1 and B2, degradation of acetate continued after majority of sulfate and U(VI) were removed (Fig. 1c1 and c2). For oleate amended microcosms, after acetate reached peak level, acetate removal was related to the sulfate concentration within the first 100 day period. In case A1, no further acetate concentration decrease was observed (Fig. 1 c1). In cases A2 and A3, acetate concentration decreased and then stabilized as sulfate consumed (Fig. 1c2 and c3). This observation indicates that acetate degradation occurred much later with oleate as substrate than with ethanol. Acetate in cases A1–A3 was found to become zero after 150 days. Methane was observed in the headspace of the microcosms. The further consumption of acetate after sulfate was consumed was likely associated with methanogenesis. Therefore, we added the CH_4 production reaction from acetate degradation at time t_8 to the complex reaction pathway model for simulation of microcosms B1 and B2:

$$C_2H_3O_2^- + H_2O \rightarrow HCO_3^- + CH_4, \quad R_8 = K_8 C_{acetate} \tag{19}$$

We did not simulated methanogenesis in A1–A3 because of lack of acetate data between days 100 and 150.

Table 4
Reaction parameter estimated for calibration of the reaction pathway models.

Microcosm	Oleate			Ethanol	
	A1	A2	A3	B1	B2
K_1 (M/day)	2.48E−01 ± 7.59E−02	2.98E−01 ± 1.25E−01	2.00E−01 ± 2.26E−02	2.00E−01 ± 4.82E−02	3.89E−01 ± 7.96E−02
K_2 (M/day)	6.09E−04 ± 2.57E−04	2.86E−03 ± 8.27E−04	1.62E−03 ± 7.85E−05	1.27E−04 ± 5.50E−04	2.09E−03 ± 2.50E−04
K_3 (M/day)	7.32E−02 ± 1.63E−01	2.79E−03 ± 1.47E−03	5.99E−03 ± 3.19E−03	3.78E−03 ± 2.77E−03	8.25E−04 ± 3.47E−04
K_4 (M/day)	4.51E−06 ± 8.02E−04	3.54E−06 ± 1.01E−03	1.00E−07 ± 1.18E−04	1.00E−07 ± 1.67E−05	1.00E−07 ± 2.35E−04
K_5 (M/day)	3.31E−02 ± 3.24E−02	1.80E−03 ± 2.30E−03	3.02E−03 ± 1.07E−03	7.83E−03 ± 1.80E−03	2.63E−03 ± 6.79E−04
t_6 (day)	–	–	–	3.60E + 01 ± 6.45E−01	5.23E + 01 ± 7.19E + 00
K_7 (M/day)	–	–	–	3.19E−01 ± 3.73E−01	6.28E−02 ± 4.75E−02
C_{oleate} (M)	3.07E−04 ± 2.14E−05	–	–	–	–

3.4. U(VI) reduction in microcosms

U(VI) concentrations decreased in both oleate and ethanol amended microcosms (Fig. 1a1–a3) but not the control microcosm (Fig. S1), indicating that the removal of U(VI) was due to microbial activities. The initiation of U(VI) removal was correlated with acetate production (i.e., degradation of oleate or ethanol) and sulfate reduction. After sulfate was consumed, the removal of aqueous U(VI) became slower (Fig. 1a1 and a2). Microcosms with higher initial sulfate had higher residual aqueous U(VI) concentrations, although more reduced U(IV) was detected in solid phase (Table 3). This was attributed to adsorption isotherm of U(VI) to sediments. Higher initial sulfate concentration also resulted higher bicarbonate concentration and raised pH (Table 3). Therefore, the higher residual aqueous U(VI) was observed in the microcosm with higher initial sulfate concentration. The influence is simulated by the aqueous complexation reactions plus surface complexation for uranium and sulfate sorption in the basic geochemistry model. More U(VI) in sediments was desorbed and reduced with higher initial sulfate concentration. Under the same initial sulfate concentration, we observed earlier and quicker U(VI) reduction in ethanol amended microcosms than in oleate amended microcosms. This was likely related to greater amount of hydrogen available with ethanol than oleate on the same COD basis (Table 1).

3.5. Model calibration

The reaction pathway model was automatically calibrated using HGC5 coupled with PEST. Model calibration results are compared to experimental data in Fig. 1. Parameter estimation results are summarized in Table 4. The model accurately tracked major features of U(VI) reduction (Fig. 1a1–a3), sulfate reduction (Fig. 1b1–b3), and acetate evolution (Fig. 1c1–c3). K_1–K_5 were estimated through calibration of sulfate, U(VI) and acetate concentration measurements without consideration of CH_4 production from acetate (Table 4). For microcosms B1 and B2, additional calibration is performed to estimate K_6 and t_6 with consideration of CH_4 production from acetate, based on the estimated K_1 through K_5 obtained from former calibration. The oleate degradation in reality was more complicated than the reaction model used in this study. In our test, oleate degradation via sulfate reduction was initially predominant. In microcosm A1 oleate was degraded associated with sulfate reduction during initial 30 days and the second increase of acetate after 60 days was likely due to degradation of some residual oleate via syntrophic acetogenesis mainly with methanogenesis. Therefore, in A1, the model assumes that only part of the total oleate (0.89 mM) was available for sulfate reduction, which represented by C_{oleate} was estimated together with the other reaction parameters.

Due to the much higher concentration of sulfate than U(VI), the consumption of acetate is mainly controlled by rate of sulfate reduction using acetate. The overall rate of sulfate reduction is influenced by the substrate degradation rate and intermediate acetate and hydrogen consumption rate. No separate data set is available to differentiate the rates of U(VI) reduction by acetate and hydrogen. However, the residual U(VI) co-existing with acetate indicates that the rate of U(VI) reduction with acetate was relatively slow. Consequently, the maximum specific rate of U(VI) reduction by acetate, K_4, was estimated to be smaller than that by hydrogen, K_5 (Table 4). Therefore, the overall rate of U(VI) bioreduction was mainly influenced by the substrate degradation rate and intermediate hydrogen consumption rate. Simulation of intermediate acetate provide better understanding of the degradation and reduction mechanisms.

As shown in Table 4, degradation rate of oleate K_1 increased as initial sulfate concentration rose from 1.09 mM (microcosm A1) to 4.92 mM (microcosm A2) but decreased as initial sulfate concentration rose further to 8.58 mM (microcosm A3). This indicates that sulfate concentration as high as 8.58 mM may cause inhibition to microbial activity.

3.6. Implementation of the results and further study

Results of this study indicated that oleate can be utilized as an electron donor source for *in situ* U(VI) reduction and immobilization. Therefore, oleate-containing edible oil may also serve as an electron donor source. The test results indicated that the degradation rate of oleate was slower than ethanol. This would be beneficial as it would help to avoid microbial clogging near an injection well and promote deep penetration of the electron donor to subsurface.

The model developed in this study simulated the test process well. However, the abiotic reduction of U(VI) to U(IV) by biogenic sulfide and reduced ferrous compounds were not specially addressed although the role of these compounds in U(VI) reduction cannot be ruled-out. It is maybe due to that the contribution of abiotic U(VI) reduction was relatively smaller than biotic reactions under the test condition in this study. If abiotic reactions were considered, more complicated model would be required. Models for U(VI) bioreduction involve many geochemical parameters, including aqueous U(VI) speciation, surface complexation and bioreaction kinetics. Therefore, for efficient *in situ* applications, sensitivity analysis is needed to simplify the models. In addition, oleate degradation and uranium reduction in reality is much more complicated than the kinetic bio-reactions specified in reaction pathway model. Uncertainty can also result from the simplification in the conceptual reaction model, which could be but not limited to: (1) when sulfate is depleted, excess acetate would be available for continued reduction of residual U(VI) by FeRB with access to bioavailable Fe(III); (2) the impact of bioreduced products on uranium immobilization; (3) reoxidation of immobilized U(IV) by dissolved oxygen or other oxidants while anaerobic or anoxic conditions was not maintained; and (4) the scale up of biogeochemical reaction. These topics are the subject of ongoing analyses.

4. Conclusion

This research mainly focused on the biogeochemical modeling of U(VI) reduction with two distinct electron donor sources, i.e., oleate and ethanol. Our study confirmed that long-chain fatty acids like oleate can serve as electron donor source for U(VI) reduction. The results of microcosm tests demonstrated that U(VI) reduction can be achieved using either oleate or ethanol as electron donor under different sulfate concentrations. Higher sulfate concentrations caused desorption of U(VI) and higher initial aqueous U(VI) concentration. Competitive sorption of U(VI) and sulfate can be accurately simulated by a basic geochemistry model that includes equilibrium aqueous complexation and surface complexation reactions. According to the aqueous speciation calculations, the dominant aqueous U(VI) species was calcium–uranyl–carbonate complex, $Ca_2UO_2(CO_3)_3$.

Degradation of oleate in the sediments proceeded more slowly than ethanol. On the same COD basis, less U(VI) was reduced to U(IV) using oleate than ethanol presumably because oleate has less hydrogen available via substrate degradation. The removal of U(VI) from the aqueous phase was mainly correlated with acetate production and sulfate reduction. Higher initial sulfate concentration led to more bicarbonate production and raised pH; and resulted in more U(VI) reduction in sediments. In oleate amended microcosms, the sulfate concentration also influenced the peak concentrations of the intermediate breakdown product acetate. Lower peak concentration was observed with lower initial sulfate concentration suggesting that oleate degradation was more dependent on sulfate reduction. Mass balance calculation shows that with increased sulfate amendment more electron donor was consumed by SRB and more U(VI) was reduced to U(IV) while less electrons were used for methane production.

A kinetic microbial reduction model incorporated with the basic geochemistry model was developed to describe the reduction of sulfate and U(VI) stimulated by oleate or ethanol. Both models track the major trend of sulfate and U(VI) reduction. The model describes the successive production and consumption of acetate, concurrent with the bioreduction of aqueous sulfate and U(VI) species. The model results imply that (1) the overall rate of sulfate reduction is influenced by the substrate degradation rate and intermediate acetate and hydrogen consumption rate and (2) the overall rate of U(VI) bioreduction is mainly influenced by both the degradation rate of organic substrates and consumption rate of hydrogen. Both mass balance calculation and model calibration show that the extent of U(VI) reduced was likely related to hydrogen available via substrate degradation. Simulation of intermediate acetate using the model provides better understanding of the degradation and reduction processes.

The kinetic microbial reduction model may be further improved by simulating biomass production and tying reaction rates to biomass rather than using a lumped rate constant. Methanogenesis could be inhibited by sulfate-reducing bacteria competing for transferred hydrogen (Abram and Nedwell, 1978). The lag of acetate degradation by methanogens maybe also due to slow growth of acetate-utilizing methanogens. It is therefore suggested that future studies consider measurement of hydrogen and biomass, and analysis of bacterial type to enable the development and testing of more comprehensive models with competition between sulfate-reducing bacteria and methanogens and growth of respective biomass. In addition, to apply oleate and other slow-release substrates to the subsurface for *in situ* bioremediation, substrate delivery strategies need to be developed to avoid well clogging and ensure efficient amendment dispersal.

Supplementary data

Supplementary data associated with this article includes description of sample location at Oak Ridge site, sulfate and U concentrations in control microcosm, and tables containing aqueous complexation reactions and surface complexation reactions considered in the model.

Acknowledgements

This research was funded by the U.S. Department of Energy, Office of Science, Office of the Biological and Environmental Research. Oak Ridge National Laboratory is managed by UT-Battelle, LLC, for the U.S. Department of Energy under Contract DE-AC05-00OR22725**.** The authors thank Kenneth Lowe and Xiangping Yin for analytical help.

Appendix A. Supplementary data

Supplementary data associated with this article can be found, in the online version, at doi:10.1016/j.jhazmat.2010.07.049.

References

[1] H.H. Tabak, P. Lens, E.D. van Hullebusch, W. Dejonghe, Developments in bioremediation of soils and sediments polluted with metals and radionuclides: 1. Microbial processes and mechanisms affecting bioremediation of metal contamination and influencing metal toxicity and transport, Rev. Environ. Sci. Biotechnol. 4 (2005) 115–156.
[2] B.E. Rittmann, P.L. McCarty, Environmental Biotechnology: Principles and Applications, McGraw- Hill, New York, 2001.
[3] D.R. Lovley, E.J.P. Phillips, Y.A. Gorby, E.R. Landa, Microbial reduction of uranium, Nature 350 (1991) 413–416.
[4] T.C. Hazen, H.H. Tabak, Developments in bioremediation of soils and sediments polluted with metals and radionuclides: 2. Field research on bioremediation of metals and radionuclides, Rev. Environ. Sci. Biotechnol. 4 (2005) 157–183.
[5] J.D. Istok, J.M. Senko, L.R. Krumholz, D.B. Watson, M.A. Bogle, A. Peacock, Y.J. Chang, D.C. White, In situ bioreduction of technetium and uranium in a nitrate-contaminated aquifer, Environ. Sci. Technol. 38 (2004) 468–475.
[6] W.-M. Wu, J. Carley, T. Gentry, M.A. Ginder-Vogel, M. Fienen, T. Mehlhorn, H. Yan, S. Carroll, J. Nyman, J. Luo, M.E. Gentile, M.W. Fields, R.F. Hickey, D.B. Watson, O.A. Cirpka, S. Fendorf, J. Zhou, P.K. Kitanidis, P.M. Jardine, C.S. Criddle, Pilot-scale in situ bioremediation of uranium in a highly contaminated aquifer: 2. U(VI) reduction and geochemical control of U(VI) bioavailability, Environ. Sci. Technol. 40 (2006) 3986–3995.
[7] W.-M. Wu, J. Carley, J. Luo, M.A. Ginder-vogel, E. Cardenas, M.B. Leigh, C. Hwang, S.D. Kelly, C. Ruan, L. Wu, J.V. Norstrand, T. Gentry, K. Lowe, T. Mehlhorn, S. Carroll, W. Luo, M.W. Fields, B. Gu, D. Watson, K.M. Kemner, T. Marsh, J. Tiedje, J. Zhou, S. Fendorf, P.K. Kitanidis, P.M. Jardine, C.S. Criddle, In situ bioreduction of uranium (VI) to submicromolar levels and reoxidation by dissolved oxygen, Environ. Sci. Technol. 41 (2007) 5716–5723.
[8] R.T. Anderson, H.A. Vrionis, I. Ortiz-Bernad, C.T. Resch, P.E. Long, R. Dayvault, K. Karp, S. Marutzky, D.R. Metzler, A. Peacock, D.C. White, M. Lowe, D.R. Lovley, Stimulating the in situ activity of Geobacter species to remove uranium from the groundwater of a uranium-contaminated aquifer, Appl. Environ. Microbiol. 69 (2003) 5884–5891.
[9] R.C. Borden, Concurrent bioremediation of perchlorate and 1,1,1-trichloroethene in an emulsified oil barrier, J. Contam. Hydrol. 94 (2007) 13–33.
[10] Y. Yang, P.L. McCarty, Comparison between donor substrates for biologically enhanced tetrachloroethene DNAPL dissolution, Environ. Sci. Technol. 36 (2002) 3400–3404.
[11] M. Quemeneur, Y. Marty, Fatty-acids and sterols in domestic wastewaters, Water Res. 28 (1994) 1217–1226.
[12] F. Roy, G. Albagnac, E. Samain, Influence of calcium addition on growth of highly purified syntrophic cultures degrading long-chain fatty acids, Appl. Environ. Microbiol. 49 (1985) 702–705.
[13] D.Z. Sousa, M.A. Pereira, A.J.M. Stams, M.M. Alves, H. Smidt, Microbial communities involved in anaerobic degradation of unsaturated or saturated long-chain fatty acids, Appl. Environ. Microbiol. 73 (2007) 1054–1064.
[14] G.N. Rees, B.K.C. Patel, Desulforegula conservatrix gen. nov., sp. nov., a long-chain fatty acid-oxidizing, sulfate-reducing bacterium isolated from sediments of a freshwater lake, Int. J. Syst. Evol. Microbiol. 51 (2001) 1911–1916.
[15] Y. Suzuki, S.D. Kelly, K.M. Kemner, J.F. Banfield, Microbial Populations Stimulated for Hexavalent Uranium Reduction in Uranium Mine Sediment, Appl. Environ. Microbiol. 69 (2003) 1337–1346.
[16] F. Zhang, W. Luo, J.C. Parker, B.P. Spalding, S.C. Brooks, D.B. Watson, P.M. Jardine, B. Gu, Geochemical modeling of reactions and partitioning of trace metals and

radionuclides during titration of contaminated acidic sediments, Environ. Sci. Technol. 42 (2008) 8007–8013.
[17] S.H. Harris, J.D. Istok, J.M. Suflita, Changes in organic matter biodegradability influencing sulfate reduction in an aquifer contaminated by landfill leachate, Microb. Ecol. 51 (2006) 535–542.
[18] J.R. Spear, L.A. Figueroa, B.D. Honeyman, Modeling reduction of uranium U(VI) under variable sulfate concentrations by sulfate-reducing bacteria, Am. Soc. Microbiol. 66 (2000) 3711–3721.
[19] Y.L. Li, H. Vali, J. Yang, T.J. Phelps, C.L. Zhang, Reduction of iron oxides enhanced by a sulfate-reducing bacterium and biogenic H_2S, Geomicrobiol. J. 23 (2006) 103–117.
[20] W. Luo, W.-M. Wu, T. Yan, C.S. Criddle, P.M. Jardine, J. Zhou, B. Gu, Influence of bicarbonate, sulfate, and electron donors on biological reduction of uranium and microbial community composition, Appl. Microbiol. Biotechnol. 77 (2007) 713–721.
[21] J.L. Druhan, M.E. Conrad, K.H. Williams, L. N'Guessan, P.E. Long, S.S. Hubbard, Sulfur isotopes as indicators of amended bacterial sulfate reduction processes influencing field scale uranium bioremediation, Environ. Sci. Technol. 42 (2008) 7842–7849.
[22] B. Hua, B. Deng, Reductive immobilization of uranium (VI) by amorphous iron sulfide, Environ. Sci. Technol. 42 (2008) 8703–8708.
[23] B. Hua, H. Xu, J. Terry, B. Deng, Kinetics of uranium (VI) reduction by hydrogen sulfide in anoxic aqueous systems, Environ. Sci. Technol. 40 (2006) 4666–4671.
[24] J. Komlos, H.S. Moon, P.R. Jaffé, Effect of sulfate on the simultaneous bioreduction of iron and uranium, J. Environ. Qual. 37 (2008) 2058–2062.
[25] J. Luo, F.-A. Weber, O.A. Cirpka, W.-M. Wu, J.L. Nyman, J. Carley, P.M. Jardine, C.S. Criddle, P.K. Kitanidis, Modeling in-situ uranium (VI) bioreduction by sulfate-reducing bacteria, J. Contam. Hydrol. 92 (2007) 129–148.
[26] J. Luo, W.-M. Wu, J. Carley, M.N. Fienen, H. Cheng, D. Watson, C.S. Criddle, P.M. Jardine, P.K. Kitanidis, Estimating first-order reaction rate coefficient for transport with nonequilibrium linear mass transfer in heterogeneous media, J. Contam. Hydrol. 98 (2008) 50–60.
[27] J.R. Spear, L.A. Figueroa, B.D. Honeyman, Modeling the removal of uranium U(VI) from aqueous solutions in the presence of sulfate reducing bacteria, Environ. Sci. Technol. 33 (1999) 2667–2675.
[28] S. Yabusaki, Y. Fang, P. Long, C. Resch, A. Peacock, J. Komlos, P. Jaffe, S. Morrison, R. Dayvault, D. White, R. Anderson, Uranium removal from groundwater via in situ biostimulation: field-scale modeling of transport and biological processes, J. Contam. Hydrol. 93 (2007) 216–235.
[29] S.D. Kelly, K.M. Kemner, J. Carley, C. Criddle, P.M. Jardine, T.L. Marsh, D. Phillips, D. Watson, W.-M. Wu, Speciation of uranium in sediments before and after in situ biostimulation, Environ. Sci. Technol. 42 (2008) 1558–1564.
[30] S.D. Kelly, W.-M. Wu, F. Yang|, C. Criddle, T.L. Marsh, E.J. O'Loughlin, B. Rave, D. Watson, P.M. Jardine, K.M. Kemner, Monitoring uranium transformations in static microcosms, Environ. Sci. Technol. (2009) (published online, December 2, 2009).
[31] S.C. Brooks, J.K. Fredrickson, S.L. Carroll, D.W. Kennedy, J.M. Zachara, A.E. Plymale, S.D. Kelly, K.M. Kemner, S. Fendorf, Inhihition of bacterial U(VI) reduction by calcium, Environ. Sci. Technol. 37 (2003) 1850–1858.
[32] D.Z. Sousa, H. Smidt, M.M. Alves, A.J.M. Stams, Syntrophomonas zehnderi sp nov., an anaerobe that degrades long-chain fatty acids in co-culture with Methanobacterium formicicum, Int. J. Syst. Evol. Microbiol. 57 (2007) 609–615.
[33] G.T. Yeh, J.T. Sun, P.M. Jardine, W.D. Burger, Y.L. Fang, M.H. Li, M.D. Siegel, HydroGeoChem 5.0: a three-dimensional model of coupled fluid flow, thermal transport, and hydrogeochem transport through variable saturatedconditions – version 5. 0., Oak Ridge National Laboratory, Oak Ridge, TN, 2004.
[34] G.-T. Yeh, Y. Fang, F. Zhang, J.T. Sun, Y. Li, M.-H. Li, M.D. Siegel, Numerical modeling of coupled fluid flow and thermal and reactive biogeochemical transport in porous and fractured media, Comput. Geosci. 14 (2010) 49–170.
[35] F. Zhang, G.T. Yeh, J.C. Parker, S.C. Brooks, M.N. Pace, Y.-J. Kim, P.M. Jardine, D.B. Watson, A reaction-based paradigm to model reactive chemical transport in groundwater with general kinetic and equilibrium reactions, J. Contam. Hydrol. 92 (2007) 10–32.
[36] J.P.E.S.T. Doherty, Model Independent Parameter Estimation, Watermark Numerical Comput. (2002).
[37] W. Dong, S.C. Brooks, Determination of the formation constants of ternary complexes of uranyl and carbonate with alkaline earth metals (Mg^{2+}, Ca^{2+}, Sr^{2+}, and Ba^{2+}) using anion exchange method, Environ. Sci. Technol. 40 (2006) 4689–4695.
[38] R. Guillaumont, T. Fanghanel, V. Neck, J. Fuger, D.A. Palmer, I. Grenthe, M.H. Rand (Eds.), Update on the Chemical Thermodynamics of Uranium, Neptunium, Plutonium, Americium, and Technetium, Elsevier, 2003, p. 918.
[39] W. Stumm, J.J. Morgan, Aquatic Chemistry, 3rd ed., John Wiley and Sons, New York, 1996, p. 1003.
[40] T.D. Waite, J.A. Davis, T.E. Payne, G.A. Waychunas, N. Xu, Uranium (VI) adsorption to ferrihydrite: application of a surface complexation model, Geochim. Cosmochim. Acta 58 (1994) 5465–5478.
[41] F. Zhang, J.C. Parker, S.C. Brooks, Y.-J. Kim, P.M. Jardine, D.B. Watson, Comparison of approaches to calibrate a surface complexation model for U(VI) sorption to weathered saprolite, Transp. Porous Med. 78 (2009) 185–197.
[42] Z.S. Kooner, P.M. Jardine, S. Feldman, Competitive surface complexation reactions of sulfate and natural organic carbon on soil, J. Environ. Qual. 24 (1995) 656–662.
[43] K. Ingvorsen, A.J.B. Zehnder, B.B. Jørgensen, Kinetics of sulfate and acetate uptake by Desulfobacter postgatei, Appl. Environ. Microbiol. 47 (1984) 403–408.
[44] D.R. Lovley, D.F. Dwyer, M.J. Klug, Kinetic analysis of competition between sulfate reducers and methanogens for hydrogen in sediments, Appl. Environ. Microbiol. 43 (1982) 1373–1379.